Recovering bits from thin air

Demodulation of bandpass sampled noisy signals for space IoT

Narayana, Sujay; Muralishankar, R.; Venkatesha Prasad, R.; Rao, Vijay S.

DOI
10.1145/3302506.3310384

Publication date
2019

Document Version
Final published version

Published in
IPSN'19

Recovering Bits from Thin Air: Demodulation of Bandpass Sampled Noisy Signals for Space IoT

Sujay Narayana*, R. Muralishankar†, R. Venkatesha Prasad* and Vijay S. Rao*
Sujay.Narayana@tudelft.nl,muralishankar@cmrit.ac.in
Delft University of Technology, the Netherlands*
CMR Institute of Technology, Bangalore, India†

ABSTRACT

Two nanosatellites recently launched into space had issues with respect to its stabilization, power and orientation. The signals were intermittent, and amateur radio enthusiasts around the globe were requested to observe the satellites so as to get their health information. As decoding the received signals required proprietary hardware (that could not be sent to everyone), amateur radio receivers recorded the signal using Software Defined Radios (SDRs) and subsampled the carrier signals to make it easy to share. The captured signals, modulated using binary Frequency Shift Keying (FSK), included noise and more importantly the frequency shifts due to Doppler, caused by the speed of the satellites (of about 7.8 km/s), thus making decoding a major challenge even for the designated proprietary receivers (failed in some cases). As the existing FSK methods did not work effectively, we were motivated by this challenge to design an effective FSK decoder that works in the presence of Doppler and noise. In this paper, we propose *Teager Energy Decoder (TED)* based on Teager Energy Operator to decode such Doppler and noise influenced sub-sampled data. TED does not need any Doppler correction mechanisms and can dynamically adapt to the changing frequency shifts. We evaluate TED using simulation as well as from the signals from those two satellites. We show that TED performs better than COTS transceivers and available GNU-radio-based solutions using SDRs. TED is low-complexity algorithm, $O(N^2)$, and has been prototyped on a low-power microcontroller. TED can be easily adopted on satellites to decode signals for space Internet of Things applications.

CCS CONCEPTS

• **Computer systems organization** → **Embedded systems**; • **Hardware** → *Digital signal processing*.

ACM Reference Format:
Sujay Narayana*, R. Muralishankar†, R. Venkatesha Prasad* and Vijay S. Rao*. 2019. Recovering Bits from Thin Air: Demodulation of Bandpass Sampled Noisy Signals for Space IoT. In *IPSN '19: Information Processing in Sensor Networks, April 16–18, 2019, Montreal, QC, Canada.* ACM, New York, NY, USA, 12 pages. https://doi.org/10.1145/3302506.3310384

IPSN '19, April 16–18, 2019, Montreal, QC, Canada

ACM ISBN 978-1-4503-6284-9/19/04...$15.00.
https://doi.org/10.1145/3302506.3310384

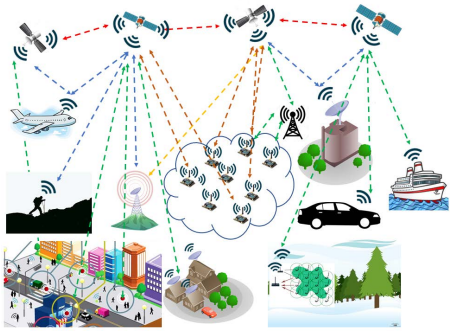

Figure 1: Concept of Space IoT

1 INTRODUCTION

Recent technological advancements have led to miniaturized wireless sensing nodes. These have become the main facilitators of the Internet of Things (IoT). In particular, the low-power, long-range communication technologies have become the key-enablers of innovation for many smart-* applications such as smart cities. With the current trend of monitoring and connecting every *thing*, coverage, connectivity and scalability are three key issues to be tackled. While cities may easily address these issues, sparsely populated areas, remote islands and harsh terrains pose challenges.

Space IoT – being pitched as a game changer for the future IoT – opens a world of new possibilities by providing a global network coverage. Space IoT is a cost-effective alternative for terrestrial IoT infrastructure in which a single/group of satellites can communicate with millions of IoT nodes and gateways directly anywhere on Earth – cities/villages, mountains, oceans, forests – at the same time [11]. Figure 1 demonstrates the concept of Space IoT. Though Space IoT is a future technology, researchers are working towards it by developing low-cost and low-power small satellite constellations [11, 12]. A commercial venture named Hiber has developed a special battery operated sensor node called *HiberBand* for their proposed system "Low-power Global Area Network" that can communicate with satellites, in a constellation, in Low Earth Orbit (around 600 km altitude or less) directly in the near future [11]. IoTEE is a EU H2020 project with a vision to provide IoT services from space by implementing a unique new communication protocol, LP(U)WAN using satellites [12]. Lacuna space is another startup that is concentrating on the development of an ultra low-cost tracking and detection service for short data messages wherein a fleet of satellites can receive data from terrestrial sensor nodes directly [18]. Similar concepts and a vision for Space IoT have also been provided in [15].

Challenges for Space IoT Communications. Though the challenges in the existing satellite communication is explored well, the concept of Space IoT adds new demands when direct communication between low-power sensor nodes and satellites is considered. Due to the large distance separation and movement of satellites (around 7.8 km/s), several existing and new challenges need to be addressed. The challenges are as follows.

i) The magnitude of Doppler effect varies over time due to the orbital dynamics and also because of the uneven curvature of Earth, thus making the demodulation of Frequency Shift Keying (FSK) signals, more challenging. Even though the Doppler shift can be theoretically modelled for specific satellite communication, usually empirical data do not conform to the derived expressions due to the influence of anomalies in satellite orientation, movements, etc.
ii) Doppler correction on nanosatellites for each 'sensor node' is very difficult and unscalable. Thus, a Doppler-correction agnostic approach is required.
iii) Miniaturized satellites generally have low gain antennas and they transmit signals at low power (around 1 W) [6]. Furthermore, signal degradation in the ionosphere and the presence of channel noise lowers the signal-to-noise ratio (SNR).
iv) Though the antenna orientation on the satellite can be changed (unlike that of the sensor node/gateway) and be omnidirectional, it cannot be pointed to a particular sensor node on Earth when thousands of sensor nodes/gateways are distributed over miles and communicate with the satellite at the same time. Furthermore, the polarization of the incoming signal may not be exactly matched with that of the receiving antenna. These issues significantly degrade the carrier-to-noise ratio (CNR) and/or SNR, thus jeopardizing the successful decoding.
v) The problem of low SNR is acute when the satellite (so the transmission antenna), is tumbling, which is typical in satellites without attitude control systems.

Motivation. Although all sub-systems of a satellite and the satellite will be tested thoroughly before launch, there is still a large scope for it to fail after deployment. Indeed, the work presented in this paper was necessitated because of a *crisis*. Two of the nanosatellites launched recently developed stabilization and orientation issues leading to intermittent and noisy telemetry. Since the satellites were not properly stabilized, they were sending intermittent data because of non-availability of continuous power and/or antenna orientation. The satellites were equipped with ON Semiconductor's AX5043 transceivers for transmitting signals down to the Earth with FSK as the modulation scheme. To maintain compatibility, the same AX5043 model transceivers were used at the designated ground stations (we call sensor nodes in our context). Because of the issues, the telemetry signals were not received by the hardware modules (equipped with AX5043) at the ground stations due to SNR lower than the required threshold mentioned in the manufacturer's datasheet. Such low CNR/SNR scenarios can occur in Space IoT frequently due to low power satellite-sensor node transmissions (both directions), the disorientation of antenna (antenna orientation on sensor node is fixed unlike on the satellite), heavy RF noise in crowded areas such as cities.

During this crisis, a few amateur radio enthusiasts around the globe were requested to help. The idea was to gather information regarding the health parameters of the satellites and command them to stabilize. When some amateur radio enthusiasts could collect some signals, to easily share the information over the Internet, the received signal was bandpass sampled. The recording rate of the signal was lower to reduce the storage space (5 GB for 1 minute recording). If the signal is stored at a lower sampling rate, i.e., bandpass sampled, a great deal of information may not be available for Doppler correction and noise minimization. The challenge was to demodulate and decode the information from the bandpass signals.

As the existing FSK methods did not work effectively, in this paper, we present a new reliable, energy-aware algorithm to decode signals resulting from direct communication between sensor nodes/gateways and satellites even when the SNR is lower than the required threshold specified by COTS transceivers. We propose a demodulation scheme for bandpass sampled FSK signals which can be decoded even in the presence of noise, Doppler effect and when the SNR is low. We propose Teager Energy based Decoding (**TED**) algorithm. TED can decode FSK modulated signals even when their SNR is as low as 1 dB. Herein, our decoding algorithm employs a non-coherent demodulation technique. In our scheme, the raw signal is filtered to attenuate lower frequencies of the received FSK signal to minimize the effect of Doppler in a non-coherent way. Later, we employed the Teager Energy Operator (TEO) for demodulating the filtered FSK signals. Our proposed solution addresses all the aforementioned challenges in decoding FSK signal. In our approach, to keep the algorithm simple, we do not compensate for the Doppler effect in the raw telemetry signal, however, we live with it, while demodulating the FSK signals in real-time. Being aware of Doppler-shifts in received signals in the wild is a difficult problem, which TED solves easily through signal detection. Indeed this work is expected to help in the proliferation of Space IoT applications, at least connecting nodes in remote/harsh environments to the IoT platforms via satellite links. In the sequel, we enlist our contributions.

Contributions. While addressing the crisis mentioned above, we built a complete receiver chain in software and tested it.

(1) We propose a novel, non-coherent approach to recover data from bandpass sampled noisy FSK signal, influenced by Doppler shift (see §4). We detect the continuous or non-continuous FSK signal in IQ (.wav) file and then decode it (see §4.1.2).
(2) We employ Teager energy operator to suppress one of the symbol frequencies while enhancing the SNR of the other. This can also be generalized for other non-coherent demodulation. To the best of our knowledge, we are the first to address the low SNR based communication issues in the context of Space IoT.
(3) We have provided end-to-end software based receiver chain starting from the detection of signals with SNR as low as 1 dB, boosting the SNR of such signals to successfully decoding them (see §4).
(4) The complexity of TED is low, $O(N^2)$, making it suitable for Space IoT.

(5) The proposed TED algorithm can be applied to demodulate FSK signals, modulated at any baud rate, from any satellite or sensor node for demodulation. Hence, it can be easily employed in any "new or existing" sensor nodes, gateways and satellites to decode the data in real-time (see §4.1.2). TED algorithm could be ported on any hardware needing only the RF front-end and a computation platform.
(6) We demonstrate the performance of TED on real-world FSK modulated signals, transmitted from satellites (see §5).

The rest of this article is structured as follows: In §2 we present the effect of SNR and Doppler shifts in satellite communication. We describe our system model and problem formulation in §3, and in §4 we present our TED algorithm. We provide evaluation of our system in §5. Finally, in §6 we list the related works on Doppler effect and FSK demodulation applicable to satellite communications and we conclude in §7.

2 EFFECT OF SNR AND DOPPLER IN SATELLITE COMMUNICATIONS

In this section, we discuss the effect of SNR and Doppler shift in satellite communication.

2.1 Effect of SNR

We explain the effect of SNR on decoding with an example. Let us consider a satellite in Low Earth Orbit (LEO) at 500 km altitude that is communicating with a single sensor node on Earth. Let us consider Texas Instruments (TI) CC1310 transceiver (one of the widely used transceivers in small satellites) is used for communication at both ends. Let us consider 435 MHz frequency for communication (one of the FCC allocated band for satellite communications). The signal from the satellite to the sensor node is FSK modulated with a frequency separation of 5 kHz. We consider the worst case for receiver parameters. The baud rate is set to 625 bps, the lowest possible in CC1310. Assuming a Noise Figure (NF) is 0 dB and the lowest available receiver sensitivity (S) of -124 dBm for bit error rate (BER) of 10^{-2}, we set the receiver bandwidth (RB) of 25 kHz (considering Doppler effect). If the satellite is transmitting the signal (with any modulation technique such as FSK, PSK, ASK) at 1 W using 5 dBi gain antenna, which is the most common in small satellites, then the required SNR on the receiver (sensor node) is given by,

$$\text{SNR(dB)} = \text{S} + 174\ \text{(dBm)} - 10\log\text{(RB)} - \text{NF}. \quad (1)$$

Substituting the parameters in (1) using CC1310's datasheet, we get SNR = 6 dB, that means, the signal power should be four times higher than the noise power for successful decoding in the best case if CC1310 is used.

To calculate the link budget, we set the gain of the antenna on the sensor node to be 2 dBi. Using Friis' equation, we get 4.7dB link margin for the SNR of 6 dB when the satellite is straight above the sensor node, i.e., at 500 km (the elevation angle in this case is 90°). In this case, CC1310 may decode the data successfully. However, as the distance between the satellite and sensor node increases (when the elevation angle is not 90°), the link budget decreases and becomes negative. For instance, when the elevation angle is around 45°, the link budget reduces to -0.8dB. This means that the sensor node will not be able to decode the data. In this case, even if the required SNR can be reduced to (say) 1.2 dB, then we get a link budget of 4 dB. Hence, decoding may not be possible with the COTS transceivers such as CC1310 or AX5043 because of the SNR threshold. Moreover, for a fixed link budget, the CNR and/or SNR may vary significantly due to RF noise on the ground (acutely in cities), signal absorption in different atmospheric layers and other RF interference.

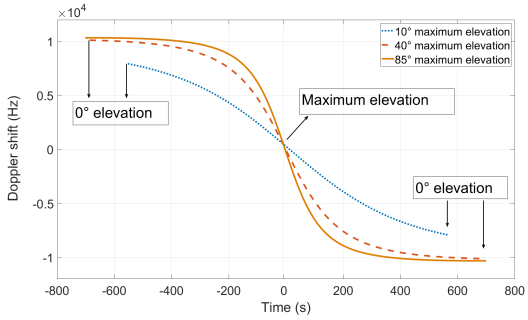

Figure 2: Doppler-Time curve for a different satellite-passes at a range of maximum elevation

2.2 Effect of Doppler Shift

Here, we describe the Doppler effect in satellite communication. The Doppler effect is the change in frequency of transmitted waves because of the relative speeds between a satellite (around 7.8 km/s in LEO) and a sensor node on Earth. For a satellite, the difference in frequency $\Delta f(t)$ between observed frequency f and emitted frequency f_o is given by,

$$\Delta f(t) = f - f_0 = \frac{\overrightarrow{v_r(t)}}{c} f_0, \quad (2)$$

where c is the velocity of the electromagnetic wave in the medium and $v_r(t)$ is the velocity of the satellite relative to the sensor node on Earth [4]. As a satellite sweeps in its orbit, the distance between the stationary observer on Earth and the satellite changes. This changes the viewing angle of the observer, which is called as elevation. $v_r(t)$, also called as range rate, is the first order derivative of slant range r of the satellite that can be predicted from Two Line Elements (TLE) of the satellite depending on the elevation angle [2][1]. The slant range is the line of sight distance between the satellite and a sensor node/gateway on Earth.

The slant range of a satellite at a specific time t in LEO can be calculated as,

$$r(t) = \sqrt{h(t)^2 + r_e^2 - 2h(t)r_e\cos\left(\lambda(t) - \theta(t)\right)}, \quad (3)$$

where $\lambda(t) = \arccos\left(\frac{r_e\cos\theta(t)}{h(t)}\right)$, with $h(t)$ being the altitude of the satellite that varies in case of non-circular orbits and also because of uneven curvature of Earth; r_e is the radius of Earth, and $\theta(t)$ is the elevation angle. For more details on calculating range rate, elevation, and Doppler shift for any satellite, we refer the reader to [2]. From (2), it is evident that the magnitude of the Doppler effect on 'M' frequencies of M-ary FSK are different. Moreover $\Delta f(t)$ is

[1] In other words, the velocity of the satellite as observed from the sensor node location changes with the elevation (angle).

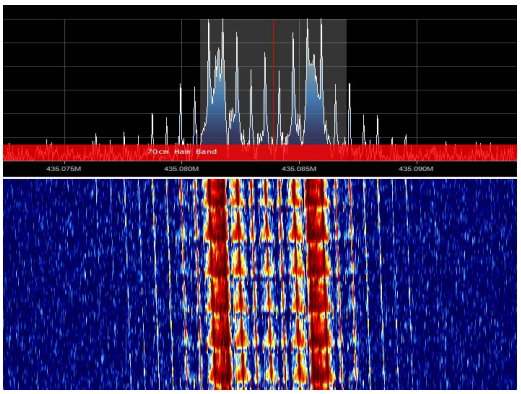

Figure 3: Telemetry reception using the software SDR#

positive if the satellite is approaching the receiver (sensor node) and is negative if it is receding.

Figure 2 shows the Doppler curve for a satellite in LEO, transmitting telemetry at 435.08 MHz, for a range of maximum elevation angles. When the elevation is maximum (maximum elevation angle) in a satellite pass the distance between the observer and the satellite is shortest. In Figure 2, the 0 s on x-axis indicates the time at which the maximum elevation is observed – Time of Closest Approach (TCA) in different passes. We observe in the plot that the curve becomes more mirrored 'S' shaped when the maximum elevation is high (85 in one case) compared to the rest, and the magnitude of Doppler shift varies with the elevation angle which is because of the range rate. We also notice in the plots that as the satellite approaches the ground station the Doppler frequency decreases. When the elevation angle is at maximum for a particularly visible pass (i.e., at 0 s), the satellite is at the closest approach vis-à-vis the observer, and the observed frequency represents the true operating frequency of the satellite. As the satellite recedes, the observed frequency starts decreasing again, causing $\Delta f(t)$ to be negative. It should be noted that the observed Doppler curve for any satellite may not coincide exactly with the analytical curve due to propagation anomalies [5]. It is to be noted that while the rate of Doppler shift is higher with high elevation the signal strength is also comparatively higher. However, with low elevation while the rate of change of Doppler shift is lower, the signal strength also reduces.

3 SYSTEM MODEL AND PROBLEM STATEMENT

In this section, we describe our system model and formulate the problem of decoding Doppler influenced noisy FSK signals. In our work, we adopt a popular model from [17] where a binary FSK modulated signal $S(t)$ is represented as,

$$S(t) = \begin{cases} \sqrt{\frac{2E_b}{T_b}} cos(2\pi f_1 t + \phi_1(t)) \text{ for bit 0} \\ \sqrt{\frac{2E_b}{T_b}} cos(2\pi f_2 t + \phi_2(t)) \text{ for bit 1,} \end{cases} \quad (4)$$

where E_b is the energy per bit in $S(t)$, the symbol duration T_b, and f_1 and f_2 are the frequencies used to represent Space (bit 0) and Mark (bit 1) in FSK. $\phi_1(t)$ and $\phi_2(t)$ are the phase terms, which

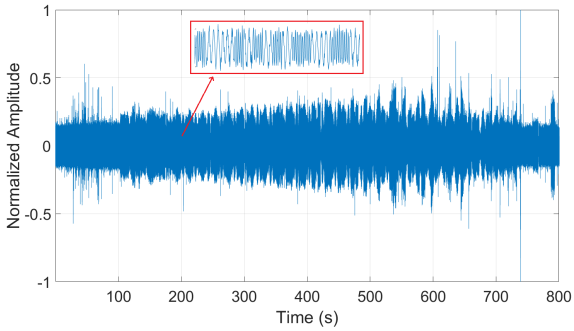

Figure 4: FSK coded signal from a satellite.

are arbitrary constants. $|f_1 - f_c| = |f_2 - f_c|$ forms the frequency deviation δf of FSK, centered at the carrier frequency f_c.

Processing high-frequency signals require more operating energy. Hence, our system model considers the signal to be bandpass sampled, down-converted to an intermediate frequency (IF) to ease the processing. This also aids in the implementation of the proposed algorithm in software on low power microcontrollers. However, the down-converted signal is also influenced by Doppler shift and noise. Here we neglect the phase component as we adopt a non-coherent approach for demodulation. Hence, we modify (4) as,

$$S(t) = \begin{cases} \sqrt{\frac{2E_b}{T_b}} cos(2\pi(f_1 t + \Delta f_1(t))) + r(t) \text{ for bit 0} \\ \sqrt{\frac{2E_b}{T_b}} cos(2\pi(f_2 t + \Delta f_2(t))) + r(t) \text{ for bit 1,} \end{cases} \quad (5)$$

where $\Delta f_1(t)$ and $\Delta f_2(t)$ are time varying Doppler shifts with f_1 and f_2, respectively, as represented by (2). $r(t)$ is a sample function of Random Process $R(t)$, which is Additive White Gaussian (AWG) with mean zero and having power spectral density $N_0/2$. To simplify the presentation, we consider the following example, using which we explain our demodulation algorithm in later sections.

Example 1. We consider a sample telemetry signal from one of our satellite, with transmission frequency $f_0 = 435.08$ MHz. The signal was recorded using a Software Defined Radio (SDR). For a better explanation, let us assume a signal with decent SNR (>3 dB) as an example such that the FSK modulation in the signal is clearly visible. However, we explain in later sections, how our algorithm also works with the signals when the SNR is very low. Figure 3 shows the online telemetry reception in SDR# software [1], indicating frequency shift when elevation was around 10°. The telemetry signal shown in Figure 4 was recorded with the sampling rate, $f_s = 50$ kHz, and the particular pass had the maximum elevation of only 16°. The signal is FSK modulated with baseband bandwidth, $B = 1.2$ kHz, and frequency deviation, $\delta f = \pm 2$ kHz. The low frequency component $f_1 = (435.08 - 0.002)$ MHz indicates bit 0 and high frequency component $f_2 = (435.08 + 0.002)$ MHz indicates bit 1. The baud rate, b, of the signal is 1200.

Using (2), the expected Doppler shift in the signal is calculated, which is shown in Figure 5. Figure 6 shows the spectrogram of the telemetry signal, displaying Mark and Space frequencies of FSK, which are affected by Doppler shift. We assume the AWGN channel. Note that the negative frequencies are folded to the positive side in the spectrogram. For a better comparison, the same has been

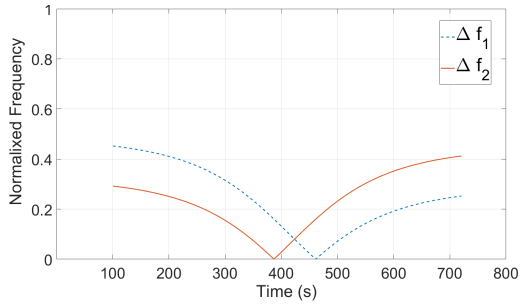

Figure 5: Expected Doppler shift in the telemetry signal

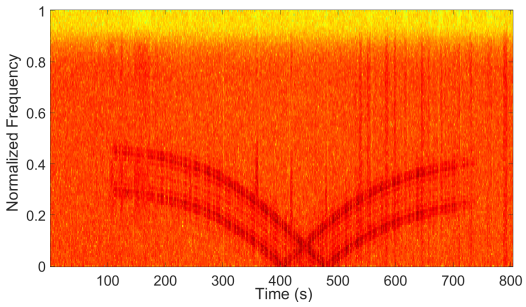

Figure 6: Spectrogram of the telemetry signal

followed in Figure 5. The y-axis is normalized with respect to $F_s/2$ = 25 kHz in both the plots. The duration of the recording is 800 s, where 0 s and 800 s correspond to elevation −1°, and 455 s corresponds to TCA of 16°. We also observe in Figure 6 that the telemetry is not continuous but intermittent because of the power fluctuations and/or frequent changes in the orientation of the satellite. Since this is the received waveform from those two distressed satellites there may also be other causes still unknown. Thus the decoding process is highly challenging.

With this example, our objective is now clear – to demodulate the signal in real-time and finally get the binary data. Further, in the process, we address two supplementary objectives (1) how to make the decoding process energy efficient; and (2) how to generalize the complete process so that it could be adopted in Space IoT applications.

4 FSK SIGNAL DETECTION AND DECODING

In this section, we explain our novel algorithm to demodulate FSK signals influenced by the Doppler shift. The approach consists of two steps: *Signal detection* – to detect the FSK signal in the telemetry, and *Signal decoding* – to demodulate the FSK signal once the FSK signal is identified. We first explain the procedure for signal detection, followed by signal decoding.

4.1 Signal detection

Before we proceed with demodulation, it is important to identify the starting position of the FSK signal that corresponds to satellite telemetry. This is challenging for the following reasons:

i) the signal from the satellite may not be present at the beginning of the recording, like in the sample telemetry signal from Example 1;
ii) the satellite communication system may be designed to send signals at specific intervals to save power (which is usually the case in small satellites);
iii) the telemetry may be discontinuous due to tumbling of satellite or other problems;
iv) in our case we had fewer samples to guess the envelope of the Doppler and also use any coherent detector.

With our search based approach for FSK modulated signals before decoding, the time consumed for demodulation is decreased especially, when the telemetry is discontinuous. Thus, signal detection performance is improved.

The first step towards signal selection is pre-processing the raw signal to filter the noise as much as possible. This helps in minimizing decoding errors such as false detection. The next step is to identify the FSK modulated signal in the telemetry. The final step is the selection of small portions/windows of the signal for demodulation, and feed it to signal decoding algorithm one after the other. Thus, the overall signal detection is done in three steps which we explain in detail:

4.1.1 Filtering. The bandwidth (BW) of an FSK modulated signal is not constant in all the telemetry signals. It varies for every pass of the satellite depending on the maximum elevation as shown in Figure 2. If $(|\Delta f_1|)_{\max}$ and $(|\Delta f_2|)_{\max}$ are the expected maximum Doppler shifts for particular maximum elevation θ_{max}, then the bandwidth of FSK modulated signal in that specific pass is given by,

$$\mathrm{BW} = 2(B + \delta f) + 2\left(\max\left((|\Delta f_1|)_{\max}, (|\Delta f_2|)_{\max}\right)\right) \quad (6)$$

Frequencies outside this bandwidth can be filtered by employing a low pass filter with cut-off frequency $BW/2$ as they do not comprise of FSK modulated signal. Considering the Example 1, we get, BW = 2(1200 + 2000) + 2 x 8800 = 24 kHz.

Applying a low-pass filter to the signal with cut-off frequency BW/2 = 12 kHz, we get the resultant filtered signal. The order of the filter was empirically chosen as 40.

4.1.2 Signal identification. The raw telemetry signal recorded by receivers also shows variation in amplitude along the time. Our novel approach towards signal identification is modelled in three dimensions – amplitude, frequency, and time – by obtaining the spectrogram of the signal. The spectrogram provides energy content (amplitude) of a signal expressed as a function of frequency and time. The vertical axis in Figure 6 represents frequency, the horizontal axis denotes time, and the amplitude over time is indicated by grey-scale (darker the grey scale, higher the amplitude). It is nothing but the windowed discrete-time Fast Fourier Transform (FFT) of a signal using a sliding window and represented in the form of a matrix containing complex values. The size of the spectrogram matrix depends on the selected length of FFT (L_{FFT}).

To identify the FSK modulated signal, the spectrogram of low-pass filtered signal is obtained first, which results in $p \times q$ matrix where p is $L_{FFT}/2$, indicating normalized positive frequencies with

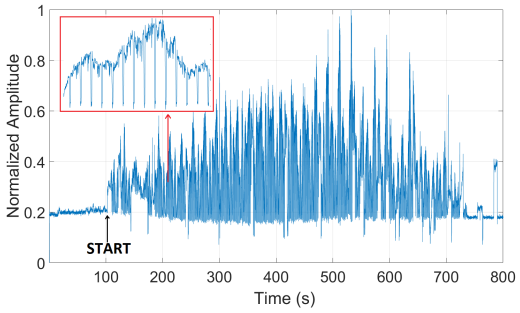

Figure 7: Envelope of the signal using spectrogram.

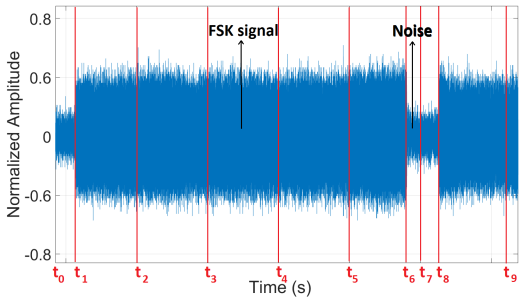

Figure 8: Window selection when FSK is continuous

respect to $F_s/2$, and q is the number of time segments in the spectrum. The $p \times q$ values are added column-wise to obtain a row-matrix having $1 \times q$ values, which represent the energy envelope of the signal at corresponding time segments. The presence of envelopes in the resultant signal indicates the FSK, whose rising edges can be identified. A continuous envelope represents the FSK and discontinuity indicates the absence of the FSK signal.

We chose 256 FFT points and non-overlapping window to obtain the spectrogram for the signal in Example 1. The values in the matrix are added column-wise to obtain a row-matrix. A low-pass filter is used to smoothen the resultant signal and the resultant waveform is shown in Figure 7. We chose the order of the filter to be 5 and cut-off frequency 1000 Hz, empirically. By setting a threshold of 0.25 (the noise floor is around 0.2) with respect to normalized amplitude, the edge detection was performed to identify the beginning of the FSK modulated signal in the spectrogram. The corresponding time stamp in the raw telemetry signal indicates the starting of the FSK modulated signal from which a window is selected for further decoding.

4.1.3 Window selection. Our approach for decoding the signal does not compensate for the Doppler effect but to work with the Doppler shift by minimizing its effect by considering each symbol period separately. We implemented a matched filter based decoding technique. Furthermore, the coefficient of the matched filter is not constant throughout the duration of the reception of telemetry due to the change in the Doppler shift. Hence, rather than considering the complete signal at once for decoding, we select windows/portions of FSK modulated signals one after the other which are then fed into the decoding algorithm for further processing.

The span of a window $\{t_i\,, t_j\}$ with $t_i < t_j$ depends on two factors:

(1) *Bit width T_b of the signal:* The window length should be a multiple of T_b; else the last bit with incomplete information will be neglected by the decoding algorithm.
(2) *Slope of Doppler curve:* The magnitude of the Doppler shift is not constant all over the signal. As we observe in Figure 2, the Doppler effect is more when θ approaches θ_{max}, the maximum elevation. The matched filter will perform better if this change is as low as possible. Hence, $\{t_i\,, t_j\}$ for a telemetry signal is a function of the slope of Doppler curve for a particular pass.

Using (2), the slope s of Doppler curve is given by

$$s_{ij} = \frac{f_0}{c}\frac{d}{dt}\left[\overrightarrow{v_r(t)}\right]_{t_i}^{t_j}, \tag{7}$$

which is always negative. The high magnitude of the slope indicates a higher Doppler shift. Hence,

$$\{t_i\,,\, t_j\} \propto |s_{ij}|^{-1}.$$

It should be noted that the Doppler cannot have slopes 0 and ∞, as zero slope indicates the absence of Doppler and infinite slope indicates an abrupt change in transmission frequency when the satellite is at the same position. For the signal in Example 1, we empirically set $t_j - t_i = 1$ s when the slope is -0.017, 200 ms when the slope is -1, and 500 ms when the slope is -57. The intermittent values are approximated using interpolation. However, the relation between the slope of the Doppler curve and window span can be generalized by fitting a curve. Hence, the window spans $\{t_i\,, t_j\}$ are chosen such that t_j - t_i = kT_b, where $k \in \{1, 2, 3\ldots\}$ and it should also confine the relation with the slope.

After the first window from the raw signal is fed into a decoding algorithm, the selection of subsequent windows depends on two cases which we explain using the Example 1. A chunk of telemetry data is shown in Figure 8. Without loss of generality, let us assume that the recording starts at t_0 and the FSK modulated signal starts from t_1. At t_6, there is a break in the FSK signal and starts again at t_9. First, the starting position t_1 of the FSK signal in the telemetry is identified using the steps described in §4.1.2. By fixing s_t to -0.3, the windows $\{t_1\,,\, t_2\}$, $\{t_2+1\,,\, t_3\}$, ... ,$\{t_5+1\,,\, t_7\}$ are calculated using (7). Since the FSK signal breaks at t_6, t_8 is identified again using the steps described in §4.1.2. The two cases affecting the window span are as follows:

Case 1: If there is a continuation in FSK signal soon after t_j, then $t_j + 1$ is chosen as t_i for next window. Hence, $\{t_1\,,\, t_2\}$, $\{t_2 + 1\,,\, t_3\}$, ...,$\{t_5 + 1\,,\, t_7\}$ form the windows in this case.

Case 2: When there is a break in FSK signal, the subsequent window begins from the next starting position of the FSK signal. Therefore, $\{t_8\,,\, t_9\}$ forms the subsequent window after $\{t_5 + 1\,,\, t_7\}$ instead of starting from $t_7 + 1$ in this case.

Thus, the raw telemetry file that is low-pass filtered (as described in §4.1.1) is fed into a signal decoding algorithm in the form of small windows after detecting the FSK signal in it.

4.2 Signal decoding

In this subsection, we explain the decoding of the FSK modulated signal using non-coherent detection. The window obtained after FSK signal detection is passed through a matched filter to suppress the low-frequency component of FSK in the signal. In our case, with

very low SNR, we propose a novel way of applying the theory of Teager Energy Operator (TEO) [13] after using the matched filter. Finally, the signal is decoded into bits. Thus, signal decoding is done in two steps which we explain in detail below.

4.2.1 Suppression of a frequency component. The matched filter is a correlation based filter where a known signal or a template is correlated with an unknown signal to detect the presence of the signal matching the template. In matched filtering, the template is a time-reversed and conjugated version of the signal, that is convoluted with the unknown signal to suppress the signal that does not match the template. One more advantage of this type of filter is that the SNR of the signal is maximized in the presence of AWGN. Hence, usage of the matched filter in signal demodulation and decoding suits Space IoT applications when SNR is low. The matched filter $h(n)$ is formulated as,

$$y(n) = \sum_{k=-\infty}^{\infty} h(n-k)x(n),$$

where $y(n)$ is the output signal and $x(n)$ is the input signal and $n \in 0, 1, 2\ldots$ The matched filter is best suited for demodulating noisy FSK signal as either low or high-frequency signal of the FSK can be considered as a template and its presence in the signal can be identified. Moreover, the probability of detection is high due to the increase in SNR. In an ideal case, the coefficient (template) of the matched filter remains the same throughout during convolution. However, this is not the case when the signal is influenced by the Doppler effect as the low and high frequencies of FSK change over time. This is one of the reasons why we choose portions of the raw telemetry signal and update the filter coefficient for each chunk. Since low frequency component $f_1 + \Delta f_1(t)$ of FSK has more Doppler effect compared to high frequency component $f_2 + \Delta f_2(t)$, we try to suppress $f_1 + \Delta f_1(t)$ using matched filter.

As explained in §4.1.3, each window starts with FSK modulated signal. To search for the high frequency component, we first take FFT of the signal over $t = \{((k-1)T_b) + 1\,,\, kT_b\}$, where $k = 0, 1, 2\ldots$. Next, we compare the magnitude of frequency between $((k-1)T_b) + 1$ and kT_b until we get one greater than the other. Finally, we choose the co-efficient of matched filter to be the signal over duration $\{((k-1)T_b)+1\,,\, \frac{(2k-1)T_b}{2}\}$, containing high frequency component[2].

Figure 9 shows a portion of the FSK modulated signal where the low frequency component is suppressed using a matched filter. It is also evident from the figure that the SNR of the matched signal is maximized. Note that if the suppression is not perceptible, then the matched filter has to be applied multiple times. The final step in the decoding process is to find the energy of the signal so that it can be decoded into bits by detecting zero-crossings.

It should be noted that, TED executes the decoding process on the modulated signal mainly in the time domain. The most important problem for decoding FSK in the frequency domain with varying Doppler shift is *finding the point of separation between carrier frequencies*. Most receivers achieve this by tracking the Doppler shifts. As we employ matched filters in TED, the filter coefficients cannot be predefined to identify the point of separation if operated in the time domain.

[2]Choosing the span over $\{((k-1)T_b) + 1\,,\, kT_b\}$ decreases the filter performance and also,$\{((k-1)T_b) + 1\,,\, \frac{(2k-1)T_b}{2}\}$ is expected to be the mirror of $\{\frac{(2k-1)T_b}{2} + 1\,, kT_b\}$.

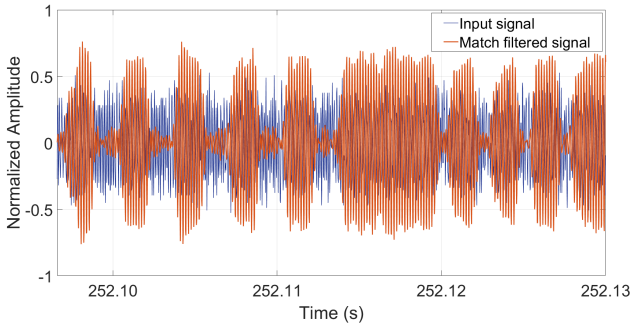

Figure 9: High frequency signal suppressed as a response to matched filter

4.2.2 Interpreting the bits. Since only one of the frequency components is retained in the signal now, it can be treated as a single component signal. Hence, the instantaneous energy of the signal at different time intervals can be used to distinguish the signal into two levels – '0' and '1'. TEO is one of the very useful tools for analyzing single component signals from the energy perspective. TEO for a discrete time signal $x(n)$ is given by,

$$\psi[x(n)] = x^2(n) - x(n-1)x(n+1) \tag{8}$$

and in the continuous case,

$$\psi[x(t)] = \dot{x}^2(t) - x(t)\ddot{x}(t) \tag{9}$$

When (9) is applied to a continuous signal of type $x(t) = Acos(\omega t)$, the resultant signal will be of type,

$$\psi[x(t)] = A^2\omega^2 \sin^2(\omega t) + A^2\omega^2 \cos^2(\omega t) = A^2\omega^2, \tag{10}$$

where $\omega = 2\pi f$.

Hence, TEO is amplitude and frequency dependent operator because of which the amplitude of the part of the signal component suppressed by the matched filter is still reduced, thus increasing SNR of the signal having retained frequency. Further explanation of the combined effect of the matched filter and TEO in the proposed approach is as follows.

A binary FSK modulated signal $S(t)$, representing low and high frequency components of FSK, respectively can be formulated as,

$$S(t) = \begin{cases} A_1 \cos \omega_1 t - \text{low frequency component and} \\ A_2 \cos \omega_2 t - \text{high frequency component,} \end{cases} \tag{11}$$

where A_1, A_2 are amplitudes of the signals, and $\omega_1 = 2\pi f_1$ and $\omega_2 = 2\pi f_2$. Also, $\omega_1 < \omega_2$. Let us choose the high frequency component as a coefficient for the matched filter. Then the output of matched filtered signal $S'(t)$ contains the components,

$$S(t) = \begin{cases} \frac{A_1}{j} \cos \omega_1 t - \text{low frequency component and} \\ A_2 \cos \omega_2 t - \text{high frequency component,} \end{cases} \tag{12}$$

where $j \in \Re$ and $j \geq 1$. Since the matched filter maximizes the SNR of the signal, the low frequency signal of FSK along with noise is suppressed by j times using a matched filter. This is evident from Figure 9.

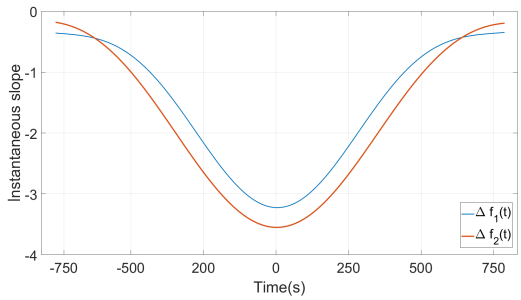

Figure 10: First order differential of Δf_1 and Δf_2

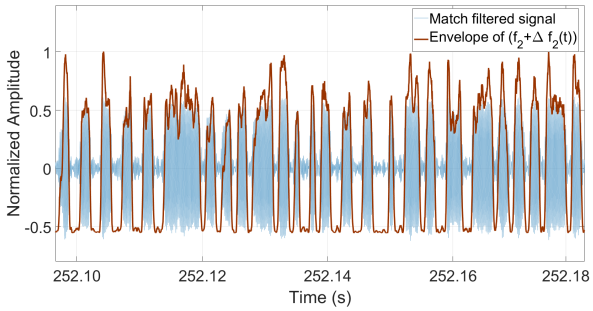

Figure 11: TEO employed on matched filtered signal

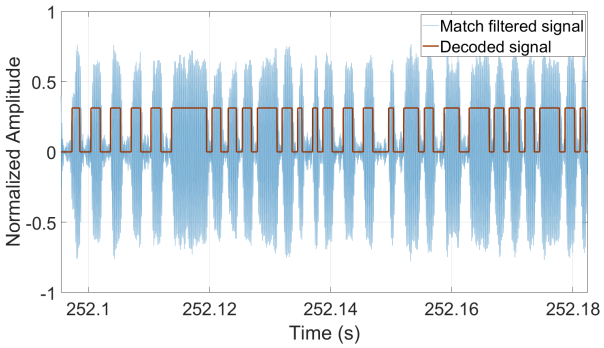

Figure 12: Decoded bits

Further, when TEO is employed, the instantaneous energy of low and high frequency components in the resultant signal becomes (using (10)),

$$\psi[S'(t)] = \begin{cases} \left(\frac{A_1}{j}\right)^2 \omega_1^2 & - \text{low frequency component and} \\ A_2^2\omega_2^2 & - \text{high frequency component} \end{cases}$$

where the low frequency component in the resultant signal is again suppressed by j times, and the energy (SNR) of the high frequency signal is increased. Hence, with the combination of the matched filter and TEO, we suppress the low frequency component in the signal along with noise.

Now, introducing the Doppler effect in (11), the FSK signal can be represented as,

$$S(t) = \begin{cases} A_1 \cos(\omega_1 t + 2\pi\Delta f_1(t)) - \text{low frequency component and} \\ A_2 \cos(\omega_2 t + 2\pi\Delta f_2(t)) - \text{high frequency component} \end{cases}$$

Applying TEO on this signal using (9), the resultant signal is,

$$\psi[S'(t)] = \begin{cases} A^2(\omega + 2\pi\Delta\dot{f_1}(t))^2 + A^2\pi\Delta\ddot{f_1}(t)\sin(2\omega t + 4\pi\Delta f_1(t)) \\ A^2(\omega + 2\pi\Delta\dot{f_2}(t))^2 + A^2\pi\Delta\ddot{f_2}(t)\sin(2\omega t + 4\pi\Delta f_2(t)). \end{cases} \quad (13)$$

The first order differential of Δf_1 and Δf_2 is shown in Figure 10. In the plots, we observe that the high frequency component Δf_2 has a higher slope than low frequency component. Hence, Δf_2 tends to zero Doppler shift faster than Δf_1. This is due to our choice of suppressing the low frequency component using a matched filter during demodulation. Further, from (13), it is evident that the output of TEO is dependent on the amplitude and frequency of the input signal. The amplitude of the low frequency component is suppressed by the matched filter, and further by TEO.

Now, applying (8) to the resultant signal obtained by employing the matched filter, we get an envelope of the matched filter output with retained frequency component as shown in Figure 11. An indication of high energy in the signal corresponds to the non-suppressed frequency component of FSK, which is $(f_2 + \Delta f_2(t))$. The zero-crossings of the envelope indicate a change in bits which can be used to represent the data in binary form as shown in Figure 12. The zero-crossings occur approximately at integral multiples of T_b and each bit must be of duration T_b. For instance, the decoded bits for the chunk of the signal shown in Figure 12 is "1100110011001100110011000000001001100 ...". It should be noted from (8) that TEO can work with just 3 samples at a time. Thus, our algorithm can dynamically adapt to varying noise-levels and Doppler shifts effortlessly.

We also observe in Figure 11 that the energy of the signal is negative when the high frequency component of FSK is not present. Here, the negative energy corresponds to the low frequency component. The negative energy in TEO is an awkward behavior for an energy operator which can be best analyzed at the extrema of the input signal, where the probability of such an event occurring is the highest [3]. These extrema are the high frequency signal (whose SNR is increased by the matched filter) of FSK and noise (AWGN + low frequency component) in the signal. We take advantage of this behavior of TEO in our algorithm for zero-crossing detection to classify the bits.

As TED uses matched filter and TEO, the computation complexity of TED is $O(N^2)$. Additionally, TED does not require a local oscillator which is required by the current chipsets. The block representation of the procedure explained above is captured in Figure 13, which is referred to as Teager Energy Decoding (TED) algorithm.

5 EVALUATION

We evaluate our TED algorithm by applying it on the signals received from those two distressed satellites. The evaluation was done using multiple telemetry signals from them. We also compare its performance with that of CC1310 and AX5043 transceivers. We choose these COTS transceivers because of their popularity, and their usage in satellite communication systems and wireless sensor nodes. Here, we consider only one-way communication – i.e., from

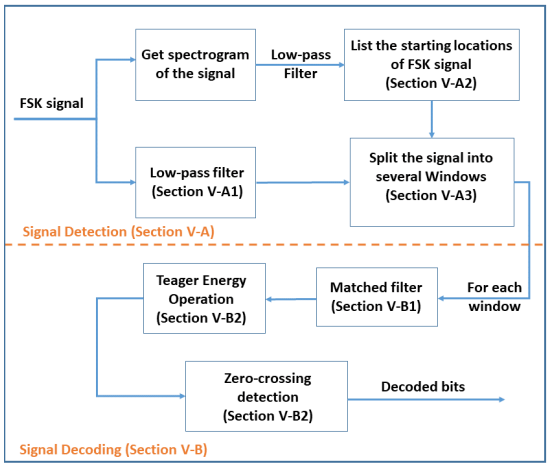

Figure 13: The proposed TED algorithm

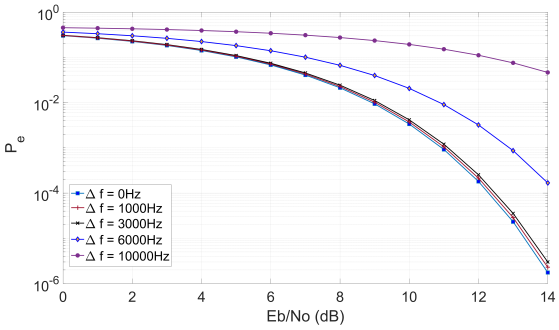

Figure 14: Bit Error Rate vs E_b/N_0 for different Δf

satellite to the sensor node as the same can be implied the other way round too.

5.1 Performance Analysis

We evaluate the performance of our algorithm using Bit Error Rate (BER). The average symbol error probability P_e for our matched filter based non-coherent, M-ary FSK modulation is in [9],

$$P_e = \sum_{i=1}^{M} \binom{M-1}{1} \frac{(-1)^{i+1}}{i+1} \exp\left[-\frac{iE_b|\cos(\mu)|\log_2 M}{N_0(i+1)}\right], \quad (14)$$

where $\mu = 2\pi\Delta f(t)$, $\Delta f(t)$ being time varying Doppler shift. For binary FSK, $M = 2$ and (14) reduces to,

$$P_e = \frac{1}{2}\exp\left(-\frac{E_b|\cos(\mu)|}{2N_0}\right) \quad (15)$$

For an M-ary FSK, the bit error probability P_b is given by,

$$P_b = \frac{M}{2M-2}P_e$$

Substituting $M = 2$, we get $P_b = P_e$ i.e., symbol error probability equal to bit error probability for binary FSK. Figure 14 shows the BER for TED algorithm for different values of E_b/No and Doppler shifts Δf. We observe in the plots that the BER changes as the Doppler shift changes. For a small increase in Doppler effect, for example, $\Delta f = 0, 1000$ and 3000, the BER is not affected much.

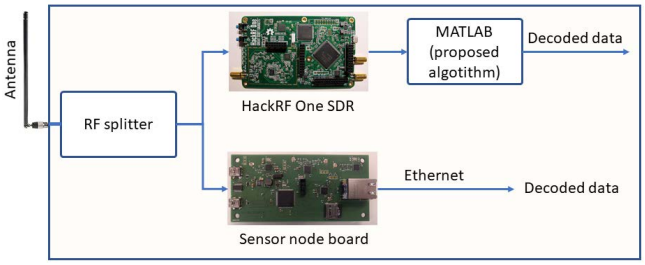

Figure 15: Experimental setup

However, a further increase in the Doppler shift affects the BER significantly.

5.2 Evaluation setup

We consider telemetry from two satellites SAT-1 and SAT-2[3], transmitting FSK modulated signals, orbiting at 505 km and 511 km altitude, respectively. Both the satellites were transmitting signals in amateur frequencies – 435.080 MHz and 437.095 MHz, respectively, at 1 W transmission power. The communication modulation scheme used was binary FSK with a frequency deviation of $\delta f = \pm 2$ kHz. The baud rate was 1.2k. Both the satellites used AX5043 transceivers. The telemetry was sent continuously down to Earth with each data packet containing 930 B. Note that the system evaluation in uplink or downlink is equivalent in our case as Doppler and SNR problems can exist on both the sides. Moreover, in downlink, we can perform the evaluation thoroughly due to extensive setup.

To extensively evaluate our algorithm, we developed a custom board, mimicking sensor nodes, housing two COTS RF transceivers – CC1310 and AX5043. The developed board is shown in Figure 15 (antennas not shown). The decoding of data for the aforementioned FSK parameters is performed by both the transceiver chips by tweaking the example source codes provided by the manufacturers. The board was also equipped with NXP's LPC1768 ARM Cortex-M3 microcontroller to configure and control the transceivers.

Alongside, we also use "HackRF One SDR" to receive raw bandpass sampled IF signal in MATLAB. Then we employ a TED algorithm to decode the data. The RF signals from the SDR were recorded at 50 kHz. The main receiver antenna, having 2 dBi gain, is connected to both SDR and the sensor node board using a splitter [4]. The overall experimental setup is shown in Figure 15.

To get the best performance from these transceivers, the Doppler compensation was done using NXP's LPC1768 ARM Cortex-M3 microcontroller on the sensor board. This was achieved by tuning the center frequency of the transceivers using the TLE information of the satellites provided by the space organizations. If this was not done, then the receiving bandwidth of both the transceivers had to be increased (as high as 25 kHz) as the center frequency was shifting because of the Doppler effect. However, Doppler compensation was

[3]We have withheld the name and telemetry packet structure of the nanosatellites to maintain confidentiality. This is not a hindrance in any way to understand the process used here.

[4]The sensor node board contains RF amplifiers to compensate the signal degradation due to RF power splitting

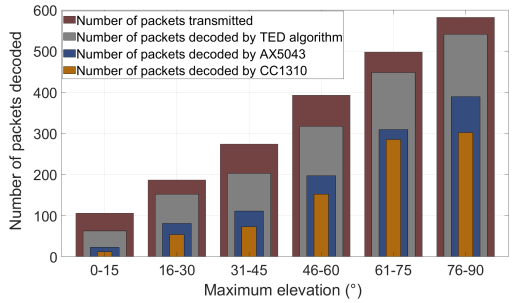

Figure 16: Number of packets decoded in different cases

not done in the case of SDR as TED algorithm performs well even in the presence of Doppler.

The telemetry was decoded online simultaneously on MATLAB (using our algorithm) as well as on the board (emulating sensor node) using both the COTS transceivers. The obtained results in all three cases (SDR, CC1310, AX5043) were compared. The number of data packets present in the telemetry of both the satellites and the count of packets decoded by TED algorithm and sensor node for different elevations of the satellite passes is shown in Figure 16. For comparison, we consider the number of packets decoded successfully without bit error, averaged over a range of maximum elevation in every satellite pass. The data plotted in the figure was obtained from averaging over 50 telemetry signals containing more than 2000 data packets in total.

We observe from the results that the TED algorithm outsmarted the COTS transceivers in decoding for all the satellite passes. Using recorded data from SDR, we later observed that the SNR of the received signals varied approximately between -2 dB and 10 dB. Whenever the SNR was above the required threshold (see 2) for CC1310 and AX5043, they decoded the signals successfully. However, the TED algorithm performed well even when the SNR was as low as 1.5 dB. It should be noted that we are not evaluating the performance between AX5043 and CC1310. Though the performance of AX5043 was better than CC1310 in our case, this may be true as the transmitter used on the satellite was also AX5043 – thus providing the matching receiver settings with the transmitter.

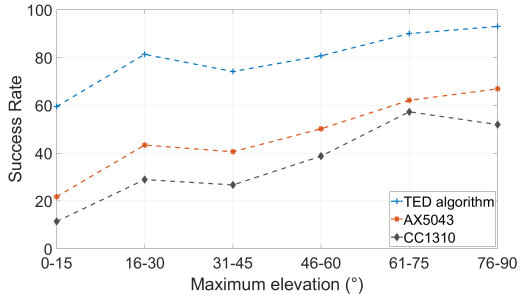

Figure 17: Success rates of decoding in different cases

To quantify the performance, we define **Success Rate** – the ratio of a total number of packets decoded without bit error and the total number of packets present in the telemetry. The Success Rates of decoding in all the cases – TED algorithm, CC1310 and AX5043 for different satellite passes are shown in Figure 17. It is evident from the figure that the TED algorithm had the Success Rate of 92.96% for maximum elevation in the range 76°-90°. While AX5043 capped at 66.8% for maximum elevation range 76°-90°, CC1310 had the maximum Success Rate of 57.23% for 61°-75° elevations. To evaluate the complexity of TED, and the feasibility of executing it on a low-power microcontroller, we ported TED onto Texas Instrument's Cortex M4 based MSP432 development board. The microcontroller operating frequency was set to 16 MHz, and the bandpass sampled raw telemetry signals from SDR were transferred to MSP432 over RS-232 using MATLAB. We observed similar performance by TED on the microcontroller to that in MATLAB. This proves that TED can be employed on low-power embedded devices such as MSP432, and be used for real-time decoding of signals. These results prove that our FSK demodulation solution can be a substitute for commercially available hardware receivers when system energy consumption and communication reliability is of concern.

5.3 Comparison with other SDR based solutions

Apart from the COTS transceivers, we also evaluate the performance of the TED algorithm with other SDR based on open source FSK demodulation techniques. We choose "demod" open source utility from cubehub[19] in combination with "multimon-ng" to decode Doppler compensated FSK signal [19]. Since it supports demodulation for only signals with the 9600 baud and 48000 sampling rate, we modified the utility to support our FSK parameters. Further, it does not take care of the Doppler shifts. Hence, we use one of the famous satellite Doppler compensation tools called "gpredict" to remove the frequency offsets before feeding the signal to demod utility. The implementation of the system is done using GNU Radio and the block diagram of modules used is shown in Figure 18. For more details on the implementation of these utilities, we point the readers to [19] and [8]. The telemetry signal from the SDR is passed

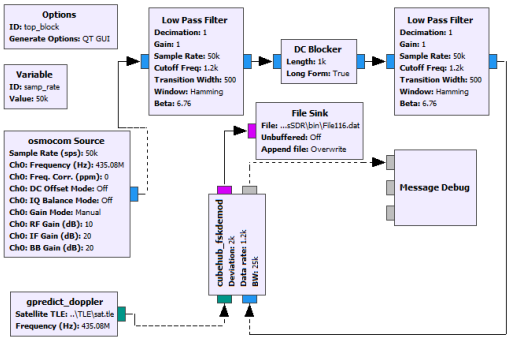

Figure 18: FSK demodulation using GNU radio

through our proposed algorithm and the GNU Radio setup. The demodulation outcomes for different satellite passes with different bit errors in every data packet are shown in Figure 19. Different telemetry signals with varying SNR, containing 2048 data packets in total are considered for the experiment. We see in the figure that the TED algorithm demonstrated the Success Rate of around 85%

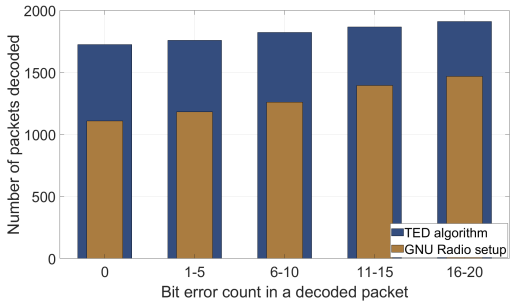

Figure 19: Number of packets decoded with bit errors

against 54% of the GNU Radio setup when no bit error is allowed in the decoded packets. However, the Success Rates of both the setups increased as the bit error count in a packet is increased. For a maximum bit error count of 20 in 930 B packet, TED algorithm decoded 1910 packets, and the GNU radio setup decoded 1467 packets.

5.4 Comparison of TED with a conventional demodulation technique

We compared the performance of TED with a conventional demodulation technique. We simulated binary FSK signals in MATLAB with the carrier frequency 435 MHz and frequency deviation of 8 kHz. The data rate was set to 1.2 kbps and 1200 subsequent bits formed a packet. These FSK signals were passed through a channel with additive white gaussian noise having varying SNRs between 0 dB and 6 dB. For every SNR consideration, we generated 100 FSK signals to find statistically stable values. Further, the Doppler shift was introduced to these noisy FSK signals to simulate the real-time scenario. These FSK signals were sampled at 50 kHz and they were demodulated using TED, and non-coherent envelope detection using a trapezoidal numeric integration method; we call it *CONV* method. Figure 20 shows the number of packets that were not successfully decoded (even a single bit error leads to the rejection of the packet) by both TED and CONV methods for FSK signals with different SNRs, and Doppler shifts of 1 kHz, 6 kHz, and 11 kHz. The results obtained in each case are the averages over 100 trials. We

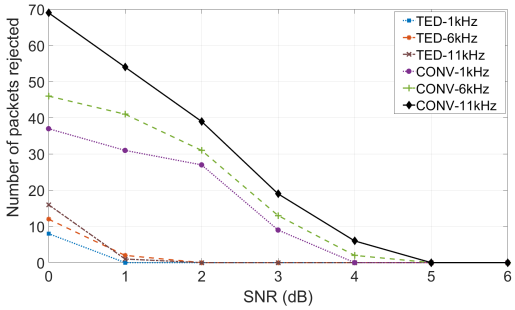

Figure 20: Number of packets that are rejected for signals with different SNRs

observe in the plots that CONV algorithm failed to decode all the signals with SNR<5 dB. TED outperformed by decoding the signals with SNR as low as 2 dB. Further decrease in SNR increases the bit errors in both the cases. The major reason for the failure in the case of the TED was that noisy coefficients of matched filter result in more bit errors as they are the templates for decoding the entire packet.

5.5 Analysis of signals with low SNR

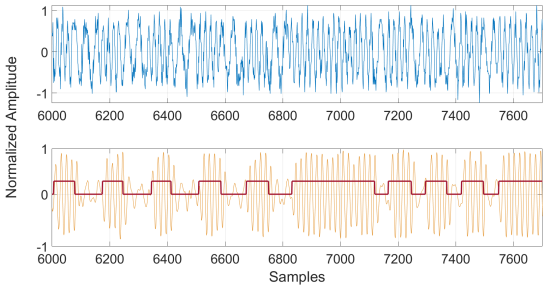

Figure 21: Signal with SNR>6 dB

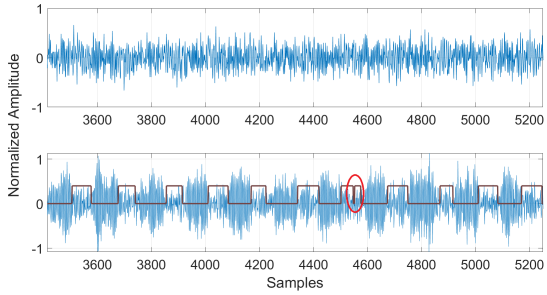

Figure 22: Signal with SNR<6 dB

We also evaluated the performance of TED against COTS receivers for telemetry signals with low SNRs. We consider a set of several raw telemetry signals, one with SNR>6 dB and the other with <6 dB (the reason for 6 dB limit being provided in §2). Figure 21 and Figure 22 show chunks of two such signals as samples. In the case of signals with SNR>6 dB, CC1310, AX5043, GNU Radio setup and TED algorithm decoded most of the packets successfully. In other cases, only TED decoded the packets. It is evident from both the figures that the combination of matched filter and TEO aids in suppressing the noise and identifying the signal. In Figure 22, we notice that TED introduced an extra bit around sample 4700 (as indicated in the figure). Such kind of bit errors was removed by comparing their bit width with the expected bit width T_b of the signal. As we noticed, the performance of TED drops when SNR falls below 1 dB or when Doppler-shift is abrupt within the time ((number of samples-per-bit)/(sampling rate)). It is around 800µs in our case. Further, higher Δf_1 implies higher $f_1 + \Delta f_1$ leading to the decreased performance of the matched filter.

6 RELATED WORK

Though there is much work done related to FSK based satellite communication in the literature, only a few works can be related to the context of Space IoT. Wannsarnmaytha, *et al.* [10], proposed a novel FSK demodulation method using Short-Term DFT (ST-DFT) analysis for LEO satellite communication systems. Using ST-DFT,

the algorithm looks for instantaneous energy spectral peak in the time-frequency plane of the signal to identify mark and space bits. However, this algorithm may not be efficient when the SNR is low. Gomadam, *et al.* [7], presented an FSK modulation and partial coherent detection scheme for time-varying channels. They considered a simple analytical model of Doppler effect for compensation. An investigation on the effects of Doppler dispersion in matched filters which use frequency translation for Doppler compensation has been provided by Remley [16]. A matched filter detector using frequency translation for Doppler compensation was implemented and analyzed statistically. A matched filter based technique was proposed in [14] to detect complicated signals subjected to a wide range of possible Doppler shifts using conjugate functions or Hilbert Transforms. A 100 tap band-pass delay line was used in conjunction with a resistor weighting matrix to synthesize signals and filter its characteristics.

An open source software "demod" makes use of open source libraries "modified multimon-ng", "doppler" and "gpredict" to decode FSK signals that can tackle Doppler problem [8, 19]. This is one of the best available solutions that can be integrated with SDRs and decode the signal online or offline. However, the software is restricted to FSK signals with the baud rate of 9600 and sampling rate of 22.05 kHz or 48 kHz. Guimaraes, *et al.* [9], explored the practical aspects of FSK modulation with non-coherent matched filter detection. The performance of a non-coherent correlator receiver and a non-coherent matched filter receiver simulated from a realistic implementation-oriented model was studied. They also discussed that the matched filter receiver can achieve superior performance under the adoption of the realistic model. However, the performance of their proposed system in the presence of Doppler effect is not discussed. To the best of our knowledge, this work is the closest to ours found in the literature, however not in the context of Space IoT. Unlike the existing work in the literature, our work provides an end-to-end FSK demodulation technique in the context of Space IoT where the SNR of received signals can be as low as 0 dB (TED decoded 90 % of the packets when SNR is around 0 dB as shown in Figure 20) for successful decoding. Additionally, the existing work entails Doppler compensation of telemetry signals before decoding them, while TED performs even in the presence of Doppler shift. With Space IoT as the primordial outlook, it is necessary to tackle the challenges of long-range, low-power communication between sensor nodes and satellites as listed in §2. In this work, we have addressed one such challenge in decoding the low SNR signals between satellite – sensor node communication in the presence of the Doppler.

7 CONCLUSION

With the proliferation of IoT applications, we envisage that satellites based IoT application is the next frontier to support remote, harsh and rural areas. In this paper, we presented a non-coherent FSK demodulation technique for bandpass sampled telemetry signals from nanosatellites. A matched filter based non-coherent detection approach is used to suppress one of the frequency components of FSK. We applied the *Teager Energy Operator* to decode the signal. The algorithm was evaluated for its performance by comparing it with a commercially available telemetry decoder. We showed that the results from TED algorithm are significantly close to the proprietary decoder and in low SNR cases, it even performed better. TED has a success rate of 92.96% compared to the nearest hardware solution that provides 66.8% decoding. We envisage that TED algorithm can be a substitute for a proven hardware in nanosatellites and also TLE is not necessary since TED is immune to Doppler shift. Another important accomplishment is that the TED algorithm can be easily used by amateur radio enthusiasts to work closely with research space missions which would bring the cost of deployment significantly less. We further plan to enhance the performance through the error correcting codes and extend the algorithm for demodulation of M-ary FSK modulated signal.

ACKNOWLEDGMENT

SCOTT http://www.scott-project.eu has received funding from the Electronic Component Systems for European Leadership Joint Undertaking under grant agreement No 737422.

REFERENCES

[1] Airspy. 2018. SDR Sharp. https://airspy.com/download/ [Online; accessed 01-Feb-2018].
[2] I. Ali, P. G. Bonanni, N. Al-Dhahir, and J. E. Hershey. 2002. *Doppler Applications in LEO Satellite Communication Systems.* Vol. 656. Springer US, Boston, MA.
[3] P. K. Banerjee and N. B. Chakrabarti. 2015. Noise sensitivity of Teager-Kaiser energy operators and their ratios. In *2015 International Conference on Advances in Computing, Communications and Informatics (ICACCI).* 2265–2271.
[4] D. E. Booth. 2004. A Doppler Compensation Scheme for RF Communications Useable on Dynamically Retargeted Projectiles. In *Proceedings for the 24th Army Science Conference.*
[5] G. Boudouris. 1960. A method for interpreting the doppler curves of artificial satellites. *Radio Engineers, Journal of the British Institution of* 20, 12 (December 1960), 933–935.
[6] J Bouwmeester and J Guo. 2010. Survey of worldwide pico and nanosatellite missions, distributions and subsystem technology. In *Acta Astronautica, Volume 67.* Acta Astronautica, 854–862.
[7] K. S. Gomadam and S. A. Jafar. 2007. Modulation and Detection for Simple Receivers in Rapidly Time-Varying Channels. *IEEE Transactions on Communications* 55, 3 (March 2007), 529–539.
[8] GPredict. 2018. Gpredict:Free, Real-Time Satellite Tracking and Orbit Prediction Software. http://gpredict.oz9aec.net/ [Online; accessed 01-Feb-2018].
[9] D.A. Guimaraes and R.A.A. de Souza. 2015. Exploring Practical Aspects of the FSK Modulation with Non-Coherent Matched Filter Detection. *Revista de Tecnologia da Informação e Comunicação (RTIC)* 5, 1 (May 2015), 22–28.
[10] S. Hara, A. Wannasarnmaytha, Y. Tsuchida, and N. Morinaga. 1997. A novel FSK demodulation method using short-time DFT analysis for LEO satellite communication systems. *IEEE Transactions on Vehicular Technology* 46, 3 (Aug 1997).
[11] Hiber. 2018. Introducing Hiberband. https://hiber.global/ [Online; accessed 01-Feb-2018].
[12] IoTEE. 2018. Internet of Things Everywhere on Earth: a satellite based M2M solution. https://cordis.europa.eu/project/rcn/207924_en.html [Online; accessed 01-Feb-2018].
[13] James F. Kaiser. 1993. Some Useful Properties of Teager's Energy Operators. In *Proceedings of the 1993 IEEE International Conference on Acoustics, Speech, and Signal Processing: Digital Speech Processing - Volume III (ICASSP'93).* IEEE Computer Society, Washington, DC, USA, 149–152. http://dl.acm.org/citation.cfm?id=1946773.1946815
[14] R. Lerner. 1960. A matched filter detection system for complicated Doppler shifted signals. *IRE Transactions on Information Theory* 6, 3 (June 1960), 373–385.
[15] S. Narayana, R. Venkatesha Prasad, V. S. Rao, and C. Verhoeven. 2017. SWANS: Sensor Wireless Actuator Network in Space. In *Proceedings of the 15th ACM Conference on Embedded Network Sensor Systems (SenSys '17).* ACM, New York, NY, USA, Article 23, 6 pages.
[16] W. R. Remley. 1966. Doppler dispersion effects in matched filter detection and resolution. *Proc. IEEE* 54, 1 (Jan 1966), 33–39.
[17] B. Sklar. 2018. Digital Communications. http://userspages.uob.edu.bh/mangoud/mohab/Courses_files/sklar.pdf [Online; accessed 01-Feb-2018].
[18] Lacuna space. 2018. Lacuna - Low-cost, simple and reliable global connections to sensors and mobile equipment. https://lacuna.space/ [Online; accessed 01-Feb-2018].
[19] A. Vahter. 2017. cubehub. https://github.com/cubehub/demod. [Online; accessed 01-Feb-2018].